SAND2013-8671C

Analysis of Gasoline Negative-Valve-Overlap Fueling via Dump Sampling

Richard R. Steeper
Sandia National Laboratories

M. Lee Davisson
Lawrence Livermore National Laboratory

Abstract

Negative valve overlap (NVO) is an operating mode that enables efficient, low-temperature gasoline combustion in automotive engines. In addition to retaining a large fraction of residuals, NVO operation also enables partial fuel injection during the recompression period as a means of enhancing and controlling main combustion. Thermal effects of NVO fueling on main combustion are well understood, but chemical effects of the products of NVO reactions remain uncertain. To address this topic, we have fabricated a dump valve that extracts a large fraction of cylinder charge at intake valve closing (IVC), yielding a representative sample of NVO products mixed with intake air. Sample composition is determined by gas chromatography. Results from a sweep of NVO start-of-injection (SOI) timings show that concentrations of the reactive species acetylene and hydrogen rise to several hundred parts-per-million as NVO SOI is retarded toward top center of NVO. Since experiments have previously demonstrated that low concentrations of acetylene seeded into the intake flow advance combustion phasing, the current results support the conclusion that NVO fueling can chemically enhance main combustion. This conclusion is further strengthened by a one-dimensional chemical kinetics simulation of main combustion that uses measured compositions as initial conditions at IVC. Comparing early and late NVO SOI, the model predicts that the hydrogen and acetylene produced by late NVO injection significantly advance the phasing of main combustion.

Introduction

The relentless drive for cleaner and more efficient engines has pushed research toward low-temperature gasoline combustion (LTGC) strategies that offer hope of achieving mandated ultra-low engine-out emissions. Such strategies often make use of auto-ignition to avoid high-temperature flames associated with spark ignition. However, this approach makes initiating and controlling LTGC a difficult challenge, especially during part-load operation.

Negative valve overlap (NVO), illustrated in Figure 1, is a well-known approach [1-3] for gaining control of LTGC on a cycle-by-cycle timescale. Several mechanisms contribute to the strategy. First, NVO can retain a large volume of residual gases for both thermal and dilution control of subsequent main combustion. Secondly, a variable fraction of each cycle's fuel can be injected during NVO's recompression period. Exothermal reaction of the NVO fuel elevates charge temperature further, contributing to the thermal control of main combustion. But depending on when and how much fuel is injected, NVO fueling can also produce reformed species that are carried over to chemically enhance main combustion.

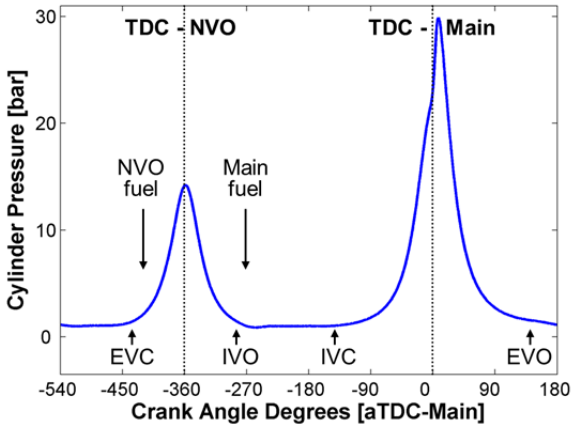

Figure 1: Typical pressure trace for fired NVO LTGC showing NVO and main portions of the cycle. Split fuel injections and valve events are labeled (exhaust/intake valve close/open). In this figure, crank angles are referenced as "after top dead center of main compression" (aTDC-Main), although in later figures, aTDC-NVO is also used as a reference when more convenient.

Many investigators [4-14] have examined thermal effects of NVO fueling on main combustion. In experiments, lean and near-stoichiometric conditions during NVO are typically selected to achieve high NVO combustion efficiencies that maximize thermal effects. Experiments designed to isolate chemical effects of NVO fueling are rarer [1,3,4,13,15,16]. By selecting oxygen-deficient or other special conditions during NVO, reforming reactions can be promoted over heat release to emphasize chemical over thermal effects. In spite of these research efforts, fundamental details of chemical enhancement of main combustion due to NVO fueling remain uncertain.

Prior experiments in our lab addressed the issue of thermal and chemical effects of NVO fueling [17]. In those experiments a small fraction of total fuel was injected during NVO and the resulting main combustion phasing was measured. Notably, we

found a distinct difference between early and late NVO fuel injection. Fuel injected early reacted relatively completely during NVO, elevating charge temperatures and advancing main combustion phasing. In contrast, fuel injected late during NVO reacted less completely, i.e., produced less heat during NVO, but it still advanced main combustion as much or more than early NVO injection. From this, we concluded that carry-over chemical species played an important role in the late NVO injection experiments. In optical experiments, we observed that late NVO fuel injection wetted the piston top, creating pool fires with conspicuous sooty flames – suggesting that the carry-over species could be products of localized rich combustion.

Further experiments identified acetylene as a likely candidate species, examining its chemical effects via seeding experiments, where NVO fuel injection was replaced by a flow of reactants into the intake air, one species at a time [18]. In that study, acetylene concentrations of 600 to 2300 ppm were found to advance main combustion phasing and elevate peak heat-release rates. The goal of the current work is to enhance understanding of NVO chemical effects by directly measuring the composition of products of NVO fueling.

Approach

Gas-Sampling System

Typically, cylinder gas sampling has relied on mini-sampling valves to extract small-volume samples that are rapidly quenched to provide time-resolved details of cylinder contents [15,16,19-21]. But the mini-samples represent only a small fraction of cylinder contents, and the external quenching process can introduce uncertainty. In contrast, several researchers have developed full-cylinder sampling devices that capture a large fraction of cylinder contents [22-24]. In the current work, we pursue this approach by developing a dump valve that takes advantage of several characteristics of NVO engine operation. First, quenching of reactions occurs naturally as the NVO products are mixed with intake air, so no special gas flows in the sampling system are necessary. And there is no need to control the quenching process since we are interested only in reactive species that persist long enough in the cycle to influence main ignition and combustion. Extraction can conveniently begin at intake valve closing (IVC) when composition is fixed, pressure is low, and piston motion assists the extraction. Finally, the sampling valve can remain open for a relatively long period (IVC to EVO) allowing a voluminous sample to be captured using a system built from commonly available hardware.

The custom dump valve illustrated in Figure 2 was designed and fabricated to fit in a conventional 14-mm threaded spark-plug port. The design mimics conventional engine valve geometry but with a scaled-down head diameter of 8 mm and lift of 3.2 mm. An automotive valve spring and retainer sit at the top of the valve stem next to a 3/16-inch Swagelok fitting providing passage for sample gases. A commercial, low-voltage solenoid at the top of the assembly is capable of actuating the valve in 4 ms. The dump valve geometry maximizes sample flow while minimizing dead volume. All parts are designed to seal both vacuum and elevated pressures while tolerating brief exhaust-gas, and steady engine-block, temperatures. Comparing motored pressure traces with and without the valve installed indicates that the leak rate through the valve is insignificant compared to, for example, engine ring blowby.

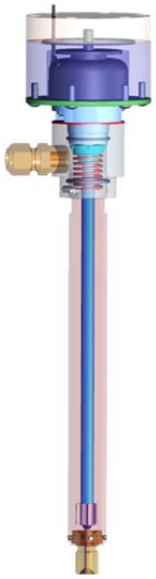

Figure 2: Schematic of the dump valve assembly.

A gas manifold (Figure 3) connects the dump valve to a 1-liter, Teflon-lined, stainless steel sample bottle and to a compact gas chromatograph (SRI Instruments Multi-Gas Analyzer #3). Pressure and temperature sensors instrument the manifold in order to monitor sampling events. Solenoid-operated isolation and vacuum valves deploy between sampling events to evacuate the manifold and minimize contamination by leaked gas. All manifold components are heated and insulated to maintain a temperature (90 °C) that is sufficient to avoid condensation of exhaust gases. The sequence of steps required to capture and analyze engine samples is described below in *Engine Operation and Sample Collection*.

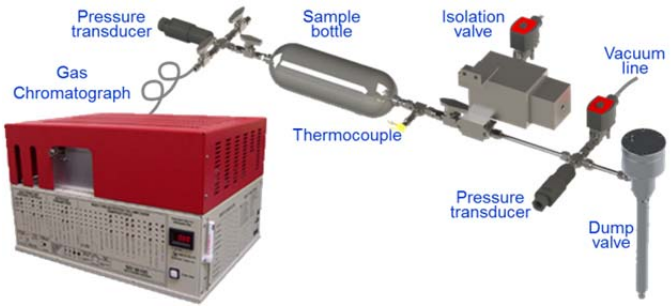

Figure 3: Schematic of dump valve, gas manifold, sample bottle, and gas chromatograph.

The gas chromatograph (GC) houses three columns and detectors capable of speciating a wide range of molecules in the NVO gas samples. The first of two flame ionization detectors (FID #1) is connected to a 60-m capillary tube (Restek MXT-1) suitable for identifying intermediate and large hydrocarbons (HC). Sensitivity of the detector is high, providing low-noise measurements of C_3 to C_8 hydrocarbons.

A second FID (FID #2) and a thermal conductivity detector (TCD) are mounted in series on a pair of packed columns (2-m Restek Hayesep-D and 2-m Restek Molecular Sieve-13x). FID

#2 is equipped with a methanizer that converts CO and CO_2 to methane in order to quantify the two. In addition, FID #2 is used to measure the C_1-C_2 hydrocarbons that are insufficiently separated on the FID #1 capillary. For the current experiments, we switched the GC carrier gas from helium to nitrogen to make the TCD sensitive to hydrogen, potentially an important species for NVO research. In this configuration, the TCD is used to quantify concentrations of hydrogen, oxygen, and water.

Figure 4 presents the three chromatograms created by sending a single engine sample through the GC. Prominent peaks are marked with red horizontal line segments. Identification and calibration of the peaks requires sending multiple samples of known composition and concentration through the GC prior to the engine experiments. For the experiments presented here, a single-point calibration was used for each of the identified species. To extract a species concentration, the area beneath its peak is calculated and multiplied by the appropriate calibration factor. Based on repeated measurements, uncertainty in reported concentrations is estimated to be better than +/- 10% for all but CO_2.

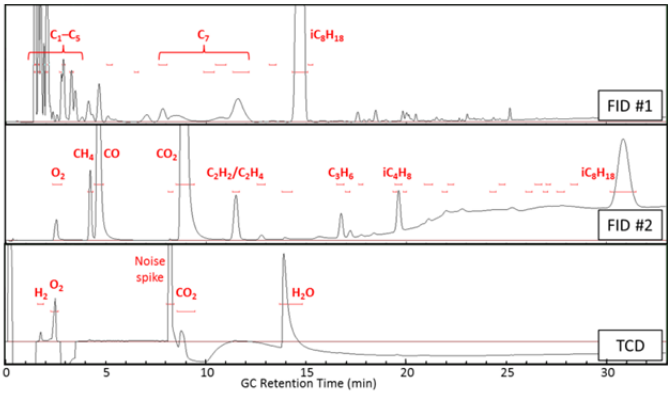

Figure 4: Sample chromatograms from the three GC detectors during a single GC run. Automated operation of the GC includes repeatably ramping carrier gas flows and temperatures to optimize separation of species. These events cause consistently timed noise spikes (adjusted to avoid signal peaks) and variations in background that are easily removed during signal integration.

Certain species are not detected by the GC, and some cannot be distinguished from other species that elute at the same time. To address this issue, several samples were transported to Lawrence Livermore National Laboratory (LLNL) for analysis on a GC equipped with a mass spectrometer. As an example, an important pair of species, acetylene and ethylene, co-elute on the Sandia GC, and they had to be separated at LLNL, as reported in the *Engine Simulation* section. Another example is formaldehyde which is difficult to measure with common detectors as well as difficult to separate with most GC columns. For these reasons, formaldehyde concentrations are not reported in this study.

Engine Operation and Sample Collection

A single-cylinder engine configured for low-temperature gasoline combustion was used for the sampling experiments. The pent-roof head houses two intake valves and a single exhaust valve, providing room for a central, 8-hole, direct injector pointing vertically toward a flat top piston. The head also includes two peripheral spark-plug ports. No spark plugs were used for the current experiments; instead, one spark-plug port housed the dump valve described above, and the second an embedded thermocouple to measure head surface temperature. For the current experiments, metal parts replaced all quartz components of this optical research engine.

Engine specifications and operating conditions used in the sampling experiments are listed in Table 1. The exhaust valve closing (EVC) and intake valve opening (IVO) events occurring 75 crank angle degrees (CAD) on either side of NVO TDC, thereby retaining a residual gas fraction of about 50%. The intake air temperature was elevated to enable compression-ignition operation at low load. To simplify sample gas speciation and facilitate modeling, iso-octane was selected as a surrogate fuel for gasoline. While holding injector trigger duration fixed, the injected mass of iso-octane drifted slowly, presumably due to variation in injector tip temperature. To obtain a constant fuel mass, the duration of the main injection was adjusted for each experiment until a Max Machinery Model 213 flow meter indicated an averaged total of 9.6 mg of fuel injected per cycle. The resulting duration of the main injection varied between 600 and 630 μs; to simplify the operating procedure, the NVO injection duration was held fixed at 165 μs. Based on prior experiments showing a significant impact of NVO injection timing on main combustion, the current sampling experiments were designed to cover a sweep of start-of-injection (SOI) timings ranging from -55 to -7 CAD aTDC-NVO.

Table 1: Engine Specifications and Operating Conditions

Displacement	0.633 liter
Bore	92 mm
Stroke	95.25 mm
Effective Compression Ratio	11.3
Intake Valve Opening, IVO	75 CAD aTDC-NVO
Intake Valve Closing, IVC	140 CAD bTDC-Main
Exhaust Valve Opening, EVO	140 CAD aTDC-Main
Exhaust Valve Closing, EVC	75 CAD bTDC-NVO
NVO duration	150 CAD
Valve Lift	3 mm
Speed	1200 rpm
Intake air temperature	393 K
Intake air pressure	100 kPa
Coolant temperature	363 K
Fuel	Iso-octane
Fuel pressure	10 MPa
Split fuel inject: NVO / Main	1.3 / 8.3 mg/cycle
NVO SOI timing sweep	-55 to -7 CAD aTDC-NVO
Overall equivalence ratio	0.6
$IMEP_G$ / COV of $IMEP_G$	190 kPa / < 4%*

* For all except the latest SOI (-7 CAD aTDC-NVO), which has a COV of 7.5%.

The following protocol enables capture of gas samples during NVO operation. Prior to beginning the sampling experiments, the gas manifold and sample bottle (Figure 3) are evacuated to

approximately 1 kPa. Once the engine is preheated, 3-4 minutes of continuous firing at the desired operating point achieves quasi-steady engine performance, as illustrated in the first frame of Figure 5. A single dump cycle is then triggered (second frame of Figure 5), and it begins the same as a continuously fired cycle, with NVO fuel being injected as usual. However, the sample cycle's main injection is unnecessary (since it comprises a known quantity of unreacted iso-octane), so it is suppressed to permit an increase in sensitivity setting of the GC detector. Near IVC, the dump valve is triggered, and cylinder contents flow through the manifold to the sample bottle. This flow causes a spike in the sample pressure (right-hand axis), and a corresponding drop in peak cylinder pressure. Following dump valve closing near EVO, the sample pressure asymptotes to about 20 kPa. The particular dump cycle in Figure 5 represents the first sample captured in the initially evacuated, 1-liter sample bottle. Thus the 20 kPa pressure indicates that approximately 200 ml of gas (at standard pressure) was collected from the engine, which is more than a third of the engine's effective displacement. Multiple dump events are performed to fill the bottle to a pressure of 1 bar, providing a cycle-averaged sample of charge composition at IVC. Following each dump cycle, the engine transitions to motoring and then, approximately 1 minute later, back to firing in preparation for the next sampling event.

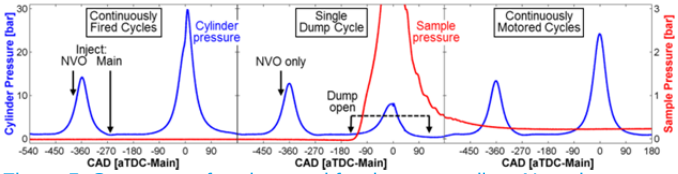

Figure 5: Sequence of cycles used for dump sampling. Note the reduced scale on the right for sample-bottle pressure.

When the sample bottle is filled to atmospheric pressure, the engine is stopped and GC analysis begins. A 25-ml sample is drawn from the sample bottle through the 2-ml GC sample loop, which then automatically injects the contents into the GC columns. Each run requires thirty minutes, and two runs are performed for each sample. Operation of the GC, from sample injection through presentation of quantitative results, is automated, so that engine experiments can be restarted once the second GC run has commenced.

Computational Approach

Cycle-temperature software [25] has been developed in house to compute bulk temperatures during NVO operation. The iterative computations account for time-varying chemical composition and thermodynamic properties, and provide estimates of temperature and heat release throughout the NVO and main portions of the cycle. In the current study, the estimates are important as a means to quantify the change in engine performance as NVO injection timing is varied.

To further assist interpretation of sampling experiment results, simulations are performed using CHEMKIN's 0-D Closed Internal Combustion Engine Simulator [26] coupled with LLNL's detailed iso-octane reaction mechanism comprising 872 species and 3796 reactions [27]. The simulation covers the main compression and power strokes as a way of assessing chemical effects of NVO products on main combustion. The simulation commences at IVC, imposing initial conditions consisting of measured cylinder pressure, estimated bulk charge temperature, and charge composition determined during the sampling experiments. Boundary conditions include measured engine wall temperatures that enable use of a Woschni submodel of wall heat transfer included in the CHEMKIN simulator.

Results and Discussion

Engine Performance

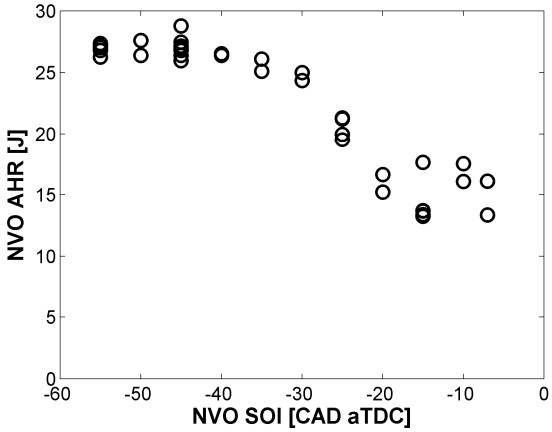

Figure 6: Apparent cumulative heat release during NVO.

A convenient metric to assess thermal effects of NVO heat release is the bulk charge temperature computed at IVC (T_{IVC}), i.e., at a point when NVO products have been mixed with intake air. Although a number of factors can influence T_{IVC} (e.g., engine exhaust temperature, residual gas fraction, and heat of vaporization of NVO fuel), Figure 7 shows that IVC temperature generally follows the same trend as NVO AHR in Figure 6. The observed downward trends of NVO AHR and T_{IVC} might lead to the expectation that late NVO injection should result in retarded main combustion. But contrary to such expectations, Figure 8 shows main heat release steadily increasing with SOI retard, and CA50 (location of 50 % mass burned point) advancing for all but the last three NVO SOI timings. As previously reported [17], we see this trend as evidence of a chemical effect of NVO fueling: given flat (or decreasing) IVC temperatures, an advance in main combustion phasing must be attributed to chemical rather than thermal effects. More specifically, localized rich reaction zones associated with late NVO fueling are hypothesized to produce reactive species that are carried over to enhance main combustion. A goal of the current work is to test this hypothesis using gas sampling to identify NVO product species.

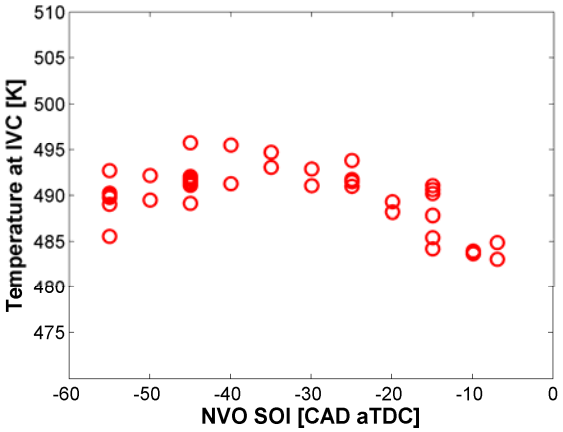

Figure 7: Estimated charge temperature at IVC.

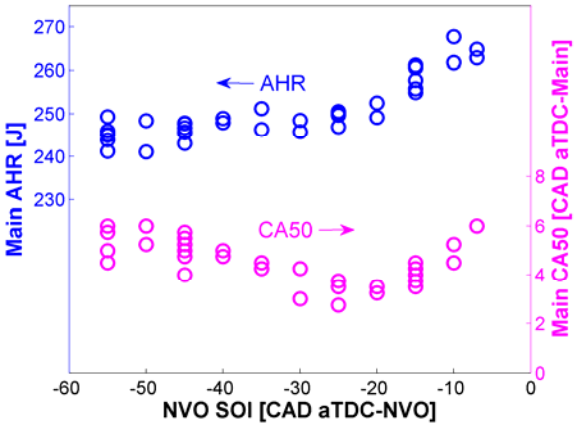

Figure 8: Apparent cumulative heat release and CA50 of main combustion.

Gas Sampling Results

Selected species concentrations representing charge composition at IVC (minus the main fuel injection) are plotted against NVO SOI timing in the following figures. Although partially obscured by scatter, the CO_2 data in Figure 9 trend generally downward, in agreement with the decreasing NVO heat release data in Figure 6. Over the same period, CO concentration increases rapidly, consistent with locally rich combustion becoming important for late injection. Note however that in prior seeding experiments, we have observed that part-per-thousand concentrations of CO do not significantly advance main combustion under these operating conditions, and therefore do not contribute to the observed advancement of CA50 in Figure 8. As a validation of measurement accuracy, the CO concentrations observed here for early and late NVO fueling match closely those measured previously in the optical engine using an in-situ laser-absorption diagnostic [28].

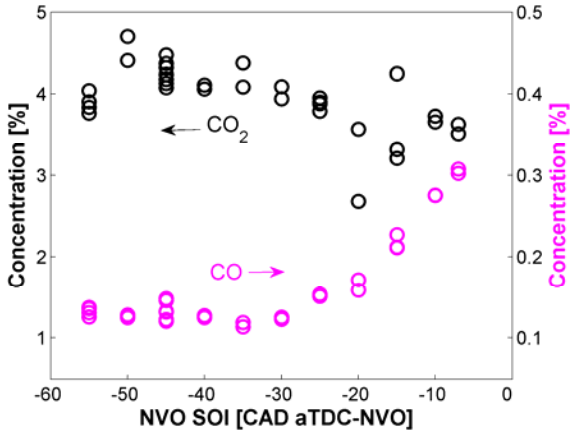

Figure 9: GC-measured concentrations of CO_2 and CO.

Several hydrocarbons identified by GC analysis are compared in Figure 10. The parent fuel iso-octane is, as expected, the most prevalent hydrocarbon in the sample. Its concentration remains fairly flat as NVO SOI is retarded, with a modest increase at the latest injection timings. Four other partial products of iso-octane oxidation are also included in Figure 10, and display similar profiles to iso-octane, but at lower concentrations. For the latest injection timing, concentrations of these species approximately double.

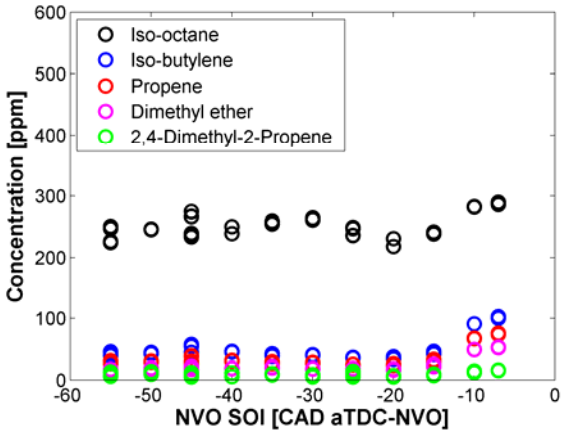

Figure 10: GC-measured concentrations of iso-octane, iso-butylene, propene, dimethyl ether, and 2,4-dimethyl-2-propene.

Three final hydrocarbon profiles, acetylene/ethylene, hydrogen, and methane, are plotted in Figure 11 with the iso-octane data repeated for scale. As stated, acetylene is of particular interest to this study, but since our GC columns do not separate acetylene and ethylene, these two species are combined in Figure 11. The reported sum of their concentrations is approximate since the GC detector response function is not identical for the two different molecules. For our purpose of describing trends during the NVO SOI sweep, this approximation is acceptable. (Later, in the *Engine Simulations* section, individual values of acetylene and ethylene concentrations are determined for a subset of the sampling experiments.)

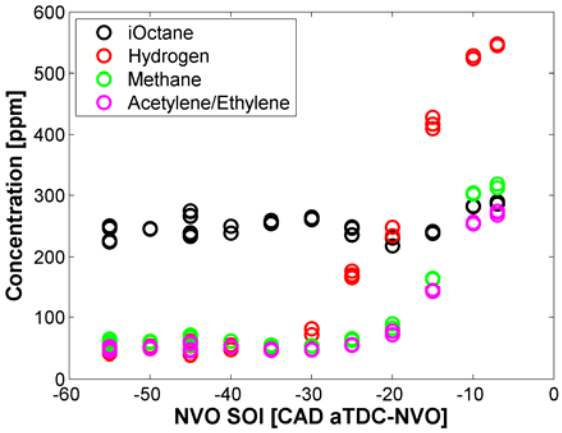

Figure 11: GC-measured concentrations of iso-octane, methane, acetylene/ethylene, and hydrogen.

Compared to the larger hydrocarbons in Figure 10, the acetylene/ethylene profile in Figure 11 displays a much stronger increase as NVO SOI is retarded. It starts early (SOI -30 CAD), and rises by more than a factor of five by the latest injection timing. Here we have evidence of NVO-produced acetylene that is carried over to the start of main compression, and combining this with the prior evidence of combustion enhancement via acetylene seeding, we gain confidence in the theory that late NVO fueling chemically affects main combustion. Note that in our acetylene-seeding experiments performed earlier, the selected concentration range started at 600 ppm, higher than values recorded in the current experiments. But since chemical effects were observed at that minimum concentration, and no effort was made to identify a lower limit for such effects, the results of the two studies are consistent, albeit somewhat incomplete.

Continuing the examination of Figure 11, methane is seen to closely follow the same trend as acetylene/ethylene. In this case, however, there is little expectation that the increase in methane contributes to the observed advance in main CA50, given the high octane rating of methane. The most striking of the species profiles in Figure 11 is hydrogen. Beginning at -30 CAD, its concentration rises by an order of magnitude as NVO SOI is retarded. Given that hydrogen and CO are primary products of rich reforming reactions, their rapid upturn in Figures 11 and 9 is entirely consistent with increasing occurrence of pool fires as NVO SOI is retarded. Further examination of the impact of the above species on main combustion is presented in the *Engine Simulations* section below.

The hydrocarbons plotted in Figures 10 and 11 represent the significant hydrocarbon species quantified by GC analysis. When all measured hydrocarbons are converted to equivalent C_3 concentrations and summed, the total concentration averages 860 ppm C_3 for early NVO injection timings (<-20 CAD). As a consistency check, this value can be compared to total hydrocarbons measured in the engine exhaust in the following way. The GC value of 860 ppm C_3 represents charge concentration at IVC minus the main fuel injection. For the same experiments, our emissions bench measures an average exhaust HC concentration of 1370 ppm C_3. In order to compare the two numbers, we first note that during the NVO period (prior to NVO fuel injection), the expected HC concentration is the same as measured in the exhaust, i.e., 1370 ppm. When NVO fuel is injected, this value will increase. If we grossly assume that NVO conversion of iso-octane approximates the conversion during main combustion, we need to multiply 1370 by the ratio (mFuelNVO+mFuelTot)/mfuelTot, where mFuelNVO is the mass of fuel injected during NVO, and mFuelTot is the total cycle fuel mass. (Strictly, a molar ratio should be used here, but the approximation is adequate since molecular weights of reactants and products are similar.) This calculation gives us an estimate of 1560 ppm HC for charge composition at the end of the NVO period (i.e., at IVO). Between IVO and IVC (where the GC measurements are made), the only process is dilution by intake air. To approximate this dilution, 1560 ppm is multiplied by the average residual gas fraction of 0.52 to get 811 ppm C_3. This 811 ppm value is an estimate, based on exhaust measurements, of HC concentration at IVC, and it is in good agreement with the direct GC measurement of 860 ppm C_3.

Two previous sampling studies with similar objectives to ours deserve comment. The work of Arning, et al. [15], made use of a mini-sampling valve connected to a GC. Sampling was triggered during late compression when charge composition should be relatively homogeneous, reducing uncertainty associated with small samples extracted near cylinder walls. While NVO operating conditions were similar to ours, a main conclusion of their study was that NVO injection effects were dominated by heat release rather than fuel reformation, which contradicts our finding of chemical effects. Several considerations may be important in explaining this discrepancy. First, the extent of NVO reformation is sensitive to the occurrence of localized rich zones associated with piston wetting. Depending on injector and head geometry (details not provided), piston wetting could have been substantially different in the earlier experiment. Second, their sampling interval was from -10 to 0 CAD aTDC-Main when temperatures could have been high enough for reactions to occur. Next, their GC measurements were uncalibrated (raw FID signal only), adding uncertainty and preventing any test of the validity of measurements. And finally, by lumping measured hydrocarbons into light and heavy categories, interesting details may have been masked. As in the earlier study, many hydrocarbons in our investigation showed only modest variation with NVO SOI timing. However, an important few species showed a dramatic response that wouldn't have been captured in the earlier work.

A second investigation by Yu, et al. [16], used a mini-sampling valve coupled with an FTIR analyzer to measure NVO composition during the compression stroke. Unlike the previous work, this study identified active species produced by NVO fueling and concluded that they enhanced gasoline auto-ignition. The quantitative measurements that were presented, as well as results of chemical kinetics simulations, highlighted important active species, including acetylene and ethylene, that are similarly identified in the current study.

Engine Simulations

The simple, single-zone model used in our computations cannot be expected to closely match the heat release of real experiments. The spatially uniform temperature of the simulation causes an overly retarded and abrupt heat release, yet results are still useful for comparing trends associated with early and late NVO injection. Figure 12 compares the main

combustion pressure trace from an early NVO SOI experiment (NVO SOI -45 CAD) with two simulations. The first simulation, labeled *Early NVO SOI*, applies initial conditions (temperatures, pressures, and species concentrations) taken from the NVO SOI -45 CAD experiment. However, to compensate for the limitations of the single-zone model, the intake temperature was increased (by 46.0 K) in order to match the experimental CA50 phasing. As expected, the simulation pressure rise rate is far too rapid compared with the experiment data, but during initial stages of heat release, the two curves are similar.

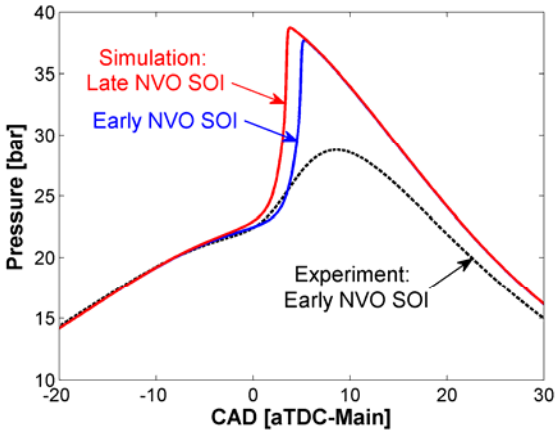

Figure 12: Comparison of experimental and simulated pressures near TDC-Main for early and late NVO SOI.

The second simulation is designed to highlight any chemical effects of late NVO fuel injection. This *Late NVO SOI* simulation elevates the concentrations of five key species to values taken from an NVO SOI -10 CAD experiment. These key species comprise the four molecules that show dramatically increasing concentrations in Figure 11, plus dimethyl ether from Figure 10. The latter is known to enhance combustion and is found with significant concentrations in our experiments. Concentrations of the key species are listed in Table 2. Concentrations of all other species in the late simulation are unchanged from the early simulation, a deliberate tactic to eliminate any effects other than those caused by the five select species.

Table 2: Key species concentrations taken from early and late NVO SOI experiments, used for simulations.

Molecule	Early NVO SOI	Late NVO SOI
Hydrogen	61.08 ppm	528.1 ppm
Methane	70.44 ppm	303.8 ppm
Acetylene	11.80 ppm	128.0 ppm
Ethylene	47.10 ppm	128.0 ppm
Dimethyl ether	21.63 ppm	49.16 ppm

Note that, unlike the *Gas Sampling Results* section, concentrations are listed separately for acetylene and ethylene in Table 2. These values were estimated by analyzing, via the LLNL GC/mass spectrometer, early and late NVO SOI samples. That analysis, shown in Figure 13, indicates that acetylene makes up approximately 20% of the combined acetylene/ethylene measurement from the early NVO SOI experiment, and 50% of the measurement from the late NVO SOI experiment.

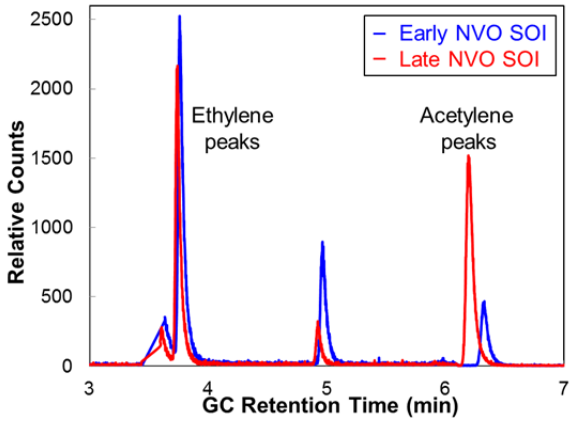

Figure 13: Relative abundance of ethylene and acetylene determined by GC/MS for early and late NVO SOI. The concentrations of the two species are determined by integrating peak areas.

Returning to the *Late NVO SOI* simulation in Figure 12, it is evident that main combustion is significantly advanced due to the elevated concentrations of the key species. The extent of this chemical effect can be better assessed in the graph of apparent heat-release rate shown in Figure 14. Here the advance in phasing is predicted to be nearly 2 CAD, with an associated increase in peak heat-release rate. Further details can be obtained by testing the effect of increasing each of the Table 2 species concentrations, one at a time. Surprisingly, acetylene alone accounts for 83% of the phasing advance seen in Figure 14. The remaining fractional advance is due to hydrogen, with the other species playing only minor roles. Interestingly, the order of magnitude increase in methane concentration associated with late NVO injection (Figure 11) actually retards slightly the predicted main combustion phasing.

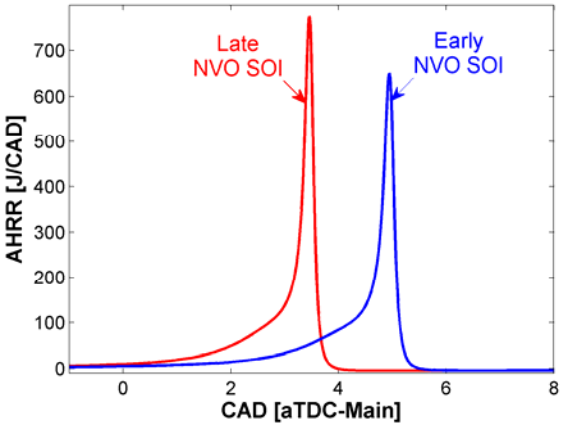

Figure 14: Simulation prediction of main combustion AHRR for early and late NVO SOI.

Summary and Conclusions

The application of a custom dump valve has demonstrated the successful sampling of NVO reaction products in an LTGC engine. Unique characteristics of NVO operation facilitate full-

cylinder sampling using relatively simple hardware. A gas chromatograph coupled to the sampling apparatus provides quantitative speciation of the NVO product samples.

The apparatus has been used to gain insight into chemical effects of NVO fueling – a strategy potentially useful for controlling LTGC auto-ignition and combustion. Comparisons of sample composition at IVC show a distinct spike in the concentration of reactive species acetylene and hydrogen as NVO-fuel-injection timing is retarded. Correlated with this increase in reactive species is a distinct advance in main combustion phasing observed during the experiments. Using measured concentrations for initial conditions, a single-zone chemical kinetics simulation predicts a similar advance in phasing. The trends observed during the experiments and simulations are consistent with observations from prior studies in our lab and elsewhere, and strengthen the conclusion that locally rich combustion associated with late NVO fueling produces reactive species that can chemically enhance main combustion.

This work has been encouraged by OEM manufacturers who seek increased authority over main combustion phasing during compression-ignition LTGC. Future work should focus on optimizing the identified chemical effects of NVO fueling. This could include an effort to identify other participating reactive species through a more detailed analysis of engine samples, as well as through more sophisticated simulation of the NVO chemistry.

References

1. Koopmans, L., Ogink, R., and Denbratt, I., "Direct Gasoline Injection in the Negative Valve Overlap of a Homogeneous Charge Compression Ignition Engine," SAE International Technical Paper 2003-01-1854, 2003, doi:10.4271/2003-01-1854.
2. Urushihara, T., Hiraya, K., Kakuhou, A., and Itoh, T., "Expansion of HCCI Operating Region by the Combination of Direct Fuel Injection, Negative Valve Overlap and Internal Fuel Reformation," SAE International Technical Paper 2003-01-0749, 2003, doi:10.4271/2003-01-0749.
3. Wermuth, N., Yun, H., and Najt, P., "Enhancing Light Load HCCI Combustion in a Direct Injection Gasoline Engine by Fuel Reforming During Recompression," SAE Int. J. Engines 2(1):823-836, 2009, doi:10.4271/2009-01-0923.
4. Aroonsrisopon, T., Werner, P., Waldman, J. O., Sohm, V., Foster, D. E., Morikawa, T., and Iida, M., "Expanding the HCCI Operation with the Charge Stratification," SAE International Technical Paper 2004-01-1756, 2004, doi:10.4271/2004-01-1756.
5. Berntsson, A. W. and Denbratt, I., "Optical study of HCCI Combustion using NVO and an SI Stratified Charge," Consiglio Nazionale delle Ricerche Technical Paper 2007-24-0012, 2007, doi:10.4271/2007-24-0012.
6. Berntsson, A. W., Andersson, M., Dahl, D., and Denbratt, I., "A LIF-Study of OH in the Negative Valve Overlap of a Spark-Assisted HCCI Combustion Engine," SAE International Technical Paper 2008-01-0037, 2008, doi:10.4271/2008-01-0037.
7. Borgqvist, P., Tunestål, P., and Johansson, B., "Investigation and Comparison of Residual Gas Enhanced HCCI using Trapping (NVO HCCI) or Rebreathing of Residual Gases," SAE International Technical Paper 2011-01-1772, 2011, doi:10.4271/2011-01-1772.
8. Hunicz, J., "An Experimental Study of Combustion Phasing Control in CAI Gasoline Engine with In-Cylinder Fuel Reforming," SAE International Technical Paper 2011-24-0052, 2011, doi:10.4271/2011-24-0052.
9. Koopmans, L. and Denbratt, I., "A Four Stroke Camless Engine, Operated in Homogeneous Charge Compression Ignition Mode with Commercial Gasoline," SAE International Technical Paper 2001-01-3610, 2001, doi:10.4271/2001-01-3610.
10. Noguchi, M., Tanaka, Y., Tanaka, T., and Takeuchi, Y., "A Study on Gasoline Engine Combustion by Observation of Intermediate Reactive Products during Combustion," SAE International Technical Paper 790840, 1979, doi:10.4271/790840.
11. Onishi, S., Jo, S. H., Shoda, K., Jo, P. D., and Kato, S., "Active Thermo-Atmosphere Combustion (ATAC) - A New Process for Internal Combustion Engines," SAE International Technical Paper 790501, 1979, doi:10.4271/790501.
12. Song, H. H. and Edwards, C. F., "Optimization of Recompression Reaction for Low-Load Operation of Residual-Effected HCCI," SAE International Technical Paper 2008-01-0016, 2008, doi:10.4271/2008-01-0016.
13. Waldman, J., Nitz, D., Aroonsrisopon, T., Foster, D., and Iida, M., "Experimental Investigation into the Effects of Direct Fuel Injection During the Negative Valve Overlap Period in a Gasoline Fueled HCCI Engine," SAE International Technical Paper 2007-01-0219, 2007, doi:10.4271/2007-01-0219.
14. Zhao, H., Peng, Z., Williams, J., and Ladommatos, N., "Understanding the Effects of Recycled Burnt Gases on the Controlled Autoignition (CAI) Combustion in Four-Stroke Gasoline Engines," SAE International Technical Paper 2001-01-3607, 2001, doi:10.4271/2001-01-3607.
15. Arning, J., Ramsander, T., and Collings, N., "Analysis of In-Cylinder Hydrocarbons in a Multi-Cylinder Gasoline HCCI Engine Using Gas Chromatography," SAE Int. J. Engines 2(2):141-149, 2010, doi:10.4271/2009-01-2698.
16. Yu, W., Xie, H., Chen, T., Li, L., Song, K., and Zhao, H., "Effects of Active Species in Residual Gas on Auto-Ignition in a HCCI Gasoline Engine," SAE International Technical Paper 2012-01-1115, 2012, doi:10.4271/2012-01-1115.
17. Fitzgerald, R. P. and Steeper, R., "Thermal and Chemical Effects of NVO Fuel Injection on HCCI Combustion," SAE Int. J. Engines 3(1):46-64, 2010, doi:10.4271/2010-01-0164.
18. Puranam, S. V. and Steeper, R. R., "The Effect of Acetylene on Iso-octane Combustion in an HCCI Engine with NVO," SAE Int. J. Engines 5(4), 2012, doi:10.4271/2012-01-1574.
19. Kölmel, A., Spicher, U., Düsterwald, R., and Wytrykus, F. M., "Analysis of Mixture Conditions Close to Spark Plug Location using a Time Resolved Gas Sampling Valve," SAE International Technical Paper 982473, 1998, doi:10.4271/982473.
20. Tsurushima, T., Shimazaki, N., and Asaumi, Y., "Gas Sampling Analysis of Combustion Processes in a Homogeneous Charge Compression Ignition Engine," IJER 1(4):337-352, 2000.
21. Yamada, H., Yoshii, M., Ohtomo, M., and Tezaki, A., "Monitoring Intermediate Species and Analysis of Their Role in HCCI Combustion," Consiglio Nazionale delle

Ricerche Technical Paper 2005-24-036, 2005, doi:10.4271/2005-24-036.
22. Hedding, G. H., Kittelson, D. B., Scherrer, H., Liu, X., and Dolan, D. F., “Total Cylinder Sampling from a Diesel Engine,” SAE International Technical Paper 810257, 1981, doi:10.4271/810257.
23. Hiroyasu, H., Nishida, K., Suzuki, M., Oda, H., Yoshikawa, S., and Arai, M., “Total In-Cylinder Sampling Experiment on Emission Formation Processes in a D.I. Diesel Engine,” SAE International Technical Paper 902062, 1990, doi:10.4271/902062.
24. Han, Y., Liu, Z., Zhao, J., Xu, Y., Li, J., and Li, K., “Impact Theory Based Total Cylinder Sampling System and its Application,” SAE International Technical Paper 2008-01-1795, 2008, doi:10.4271/2008-01-1795.
25. Fitzgerald, R. P., Steeper, R., Snyder, J., Hanson, R., and Hessel, R., “Determination of Cycle Temperatures and Residual Gas Fraction for HCCI Negative Valve Overlap Operation,” SAE Int. J. Engines 3(1):124-141, 2010, doi:10.4271/2010-01-0343.
26. Reaction Design, CHEMKIN-PRO, http://www.reactiondesign.com/products/open/chemkin.html, 2012.
27. Lawrence Livermore National Laboratories, Iso-Octane Chemical Kinetic Mechanism, https://www-pls.llnl.gov/?url=science_and_technology-chemistry-combustion-iso_octane_version_3, 2012.
28. Fitzgerald, R. P. and Steeper, R. R., “Application of a Tunable-Diode-Laser Absorption Diagnostic for CO Measurements in an Automotive HCCI Engine,” SAE Int. J. Engines 3(2):396-407, 2010, doi:10.4271/2010-01-2254.

Contact Information

Corresponding author:
Richard R. Steeper
Sandia National Laboratories
steeper@sandia.gov

Acknowledgements

Research at Sandia was supported by the U.S. Department of Energy, Office of Vehicle Technologies. Sandia is a multiprogram laboratory operated by Sandia Corporation, a Lockheed Martin Company, for the United States Department of Energy’s National Nuclear Security Administration under contract DE-AC04-94AL85000. Research at Lawrence Livermore National Laboratory was performed under Contract DE-AC52-07NA27344. We gratefully acknowledge extensive technical discussions with General Motors Research staff, and the assistance of Sal Birtola, Ken Hencken, and Sam Fairbanks in designing and fabricating the dump-valve sampling system.

Definitions/Abbreviations

AHR/AHRR	Apparent heat release/rate
aTDC/bTDC	After / before top dead center
-NVO/-Main	Pertaining to NVO/Main portion of cycle
CA50	Crank angle at 50 % mass burn point
CAD	Crank angle degree
COV	Coefficient of variation
EVC/EVO	Exhaust valve close / open
FID	Flame ionization detector
GC	Gas chromatograph
HCCI	Homogenous charge compression ignition
HR	Heat release
IMEPG	Gross indicated mean effective pressure
IVC/IVO	Intake valve close / open
LTGC	Low-temperature gasoline combustion
MS	Mass spectrometer
NVO	Negative valve overlap
OEM	Original equipment manufacturers
SOI	Start of injection
TCD	Thermal conductivity detector
T_{IVC}	Intake-valve-closing temperature